Full Articles

Sorption and cytotoxicity of zinc on hydroxyapatite

A. V. Severin,[a] M. A. Orlova,[a,b] E. S. Shalamova,[a] T. P. Trofimova,[a,b] and I. A. Ivanov[a]*

[a]Department of Chemistry, M. V. Lomonosov Moscow State University, Building 3, 1 Leninskie Gory, 119992 Moscow, Russian Federation. E-mail: orlova.radiochem@mail.ru
[b]Dmitry Rogachev National Research Center of Pediatric Hematology, Oncology, and Immunology, 1 ul. Samory Mashela, 117997 Moscow, Russian Federation

The preparation, physicochemical properties, and cytotoxicity of zinc-containing hydroxyapatites (HAP) were considered for further using HAP as carriers for zinc-containing drugs and radiopharmaceuticals.

Key words: hydroxyapatite, nanoparticles, zinc.

Diagnosis and therapy of oncological diseases require novel medical technologies and development of already known ones among which the role of radiopharmaceuticals (RPCs) is being enhanced. They are actively used in diagnostics and, to a lower extent, in therapy. The field of theranostics combining both these possibilities is being developed in the recent time. All these trends demand a great variety of radionuclides with diverse properties and vectors capable of isotope delivery to biotargets. In the case of therapeutic use, there is an additional task of prolonged action of drugs, which can be achieved by slower releasing of the radionuclide from the carrier or a low decay constant for a complex radionuclide—vector (spacer). A more interesting variant is the preparation of complicated complexes in which radionuclide is simultaneously linked to the carrier and vector. The carrier can be inert acting as an isotope-emitting scaffold or active: an organic molecule with therapeutical functions. Zinc and copper radionuclides (in particular, ^{69m}Zn and ^{64}Cu) able to various geometries of complex formation[1] are especially promising as metal isotopes, and hydroxyapatite (HAP) can act as an inert carrier. Usual zinc-containing drugs along with RPCs can also be delivered by HAP. Hydroxyapatite is widely used as a biocompatible material in many fields of

Published in Russian in *Izvestiya Akademii Nauk. Seriya Khimicheskaya,* No. 1, pp. 0009—0015, January, 2017.
1066-5285/17/6601-0009

medicine[2,3] and mainly for contact with bone tissue because of its similarity with mineral bone.[4] The general formula of HAP is $Ca_{10}(OH)_2(PO_4)_6$,[5] which is the main inorganic mineral component of the bone and dental tissues of man and mammals. Such properties as biocompatibility, bioresorbability, and bioactivity are also characteristic of HAP. The composition of biohydroxyapatite deviates from stoichiometry: its structure is calcium-deficient (the calcium to phosphorus ratio in stoichiometric HAP is 1.67) and contains significant amounts of carbonate anions.[3] The formula of biohydroxyapatite is as follows: $Ca_{10-x-y/2}(HPO_4)_x(CO_3)_y(PO_4)_{6-x-y}(OH)_{2-x}$.

There are various modification technologies for the preparation of nanocomposite, nanofiber, and nanostructural frameworks based on HAP for drug delivery.[6] The main questions for them are delivery ways and mechanisms by which nano-HAP/polymer aggregates affect cell proliferation and differentiation. The particle size and shape of HAP and its derivatives are substantial factors influencing on proliferation and cytotoxicity,[7] although numerous *in vitro* and *in vivo* studies showed that synthetic HAP had no local or system toxicity.[8,9] Moreover, nano-HAP can inhibit the growth of some types of cancerous cells with a minimum effect on healthy cells.[10] In the first step of the study of the prospects of using nano-HAP prepared by various methods as a carrier for zinc-containing drugs, one should consider the sorption kinetics of zinc on HAP, choice of the procedure for preparing zinc-containing HAP, and its cytotoxicity compared to native HAP. The present work is devoted to this consideration.

The biological functions of synthetic HAP are determined by its particle size, morphology, crystallinity, and composition depending, in turn, on the used precursors and synthesis process. Depending on the method of synthesis, one can obtain HAP samples differed in morphology and crystal size and, as a result, in properties. A similar effect is exerted by impurities (Fig. 1). The methods for synthesis of HAP are well described.[11—17]

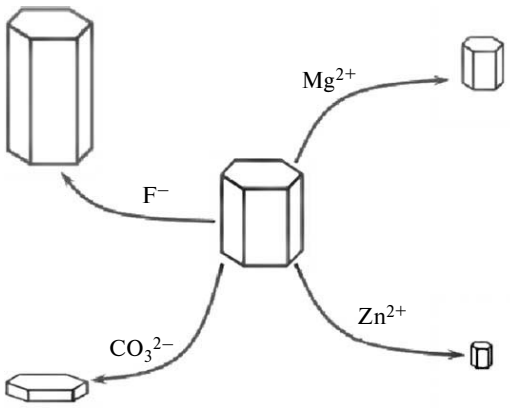

Fig. 1. Influence of some impurities on the hydroxyapatite structure.[24]

Metal ions can be introduced into HAP by adsorption binding with HAP nanoparticles or by providing the participation of metal ions in the synthesis of the HAP itself adding zinc to the reaction sphere.[16] For example, the addition of phosphoric acid to a mixture of calcium hydroxide and zinc nitrate tetrahydrate ((Zn + Ca)/P = 1.67) gave[18] oval crystals with average sizes of 15×50 nm and a zinc content of 1.2% of the HAP weight. At high concentrations zinc can enter the structure of hydroxyapatite substituting calcium to form the tetrahedral coordination mode. In this case, the phase obtained becomes more amorphous than that of pure HAP. However, the main problem of this study is the use of the salt synthesis of HAP, which imposes certain constraints on the purity of the synthesized compound and results in the necessity to be saved from the deteriorating salt background. The procedure for synthesis of superpure 2D crystalline HAP with the very high bioactivity has previously[13] been developed, which increases the proliferative ability of osteoblasts. This procedure was chosen for the synthesis of Zn-HAP in this work. The choice of the introduced zinc concentration (5 and 15 mol.% of the calcium content) was based on the published data[18,19] indicating that at the concentration >20 mol.% zinc begins to form the intrinsic phase. In addition, zinc becomes toxic at high concentrations.

Experimental

Synthesis of HAP. Hydroxyapatite (HAP-0) was synthesized using a described procedure.[13,20] A weighed sample of calcium oxide was introduced into distilled water with continuous stirring in a special reactor, and then a 30% solution of orthophosphoric acid (reagent grade, Russia) was added gradually at the molar ratio Ca/P = 1.67, which corresponds to the stoichiometry of HAP. The amounts of all reagents used were selected in such a way that a 5% (by the solid phase weight) suspension of the product was used. A 30% solution of orthophosphoric acid was added to the reaction mixture with a peristaltic pump, monitoring the course of HAP formation by a change in the pH of the solutions (Pracitronic MV88 pH meter, Germany, accuracy 0.01 pH). The reaction is considered completed after the addition of a stoichiometric amount of orthophosphoric acid or when pH 6—7 is attained.[19] The synthesis was carried out at room temperature (~20 °C). A portion of the obtained suspension was sampled for studying by transmission electron microscopy and for MTT test. The content of the solid phase in the suspension was determined gravimetrically, and the residual calcium content in the mother liquor was analyzed by ICP-AES (atomic emission spectroscopy with inductively coupled plasma) on an Optima 2100 DV instrument (Perkin—Elmer, USA). To perform X-ray phase analysis, the solid phase was separated by centrifugation, and the residue was dried at 80 °C to a constant weighed, powdered in a porcelain mortar, and kept in glass weighing bottles with ground caps until analyzing.

To obtain a HAP sample treated under hydrothermal conditions (HAP-0_{HT}), a similar synthesis was carried out at the end of which the suspension was heated to 90 °C without boiling and kept under these conditions for 4 h. Then sampling for physicochemical analysis was performed.

Introduction of zinc ions in the synthesis of HAP. For the introduction of Zn^{2+} ions in the synthesis of HAP, a weighed sample of zinc oxide (reagent grade) corresponding to the calculated molar ratio Zn/Ca = 5 (15 mol.%) was dissolved in orthophosphoric acid in an individual weighing bottle with continuous magnetic stirring. The obtained solution of zinc dihydrophosphate was added dropwise to a suspension of $Ca(OH)_2$ with an automated doser with continuous stirring. residues of the solution with Zn^{2+} were washed down with a minor amount of distilled water (~5 mL) and added to the reaction mixture. Then automatic supply of orthophosphoric acid was switched on, and the synthesis was continued slowly with stirring as described above. The presumable reaction scheme is the following:

$$Zn(H_2PO_4)_2 + Ca(OH)_2 + H_3PO_4 \longrightarrow$$

$$\longrightarrow Ca_{5-x}Zn_x(PO_4)_3OH + H_2O.$$

As in the case with pure sample of HAP-0, samples were taken for analysis (HAP-Zn_1 and HAP-Zn_2). Some dried samples were annealed in muffle furnace in air at 900 °C for 3 h (samples of HAP-Zn_{1T} and HAP-Zn_{2T}) and studied by X-ray phase analysis (XRD).

Physicochemical methods for studying the samples. The XRD patterns of all samples were obtained on a DRON-3 automated X-ray diffractometer. The measurements were carried out with the Co-Kα (λ = 0.1790 nm) or Cu-Kα electrode (λ = 0.154178 nm). The XRD pattern for pure HAP subjected to the thermal treatment (1100 °C, 3 h, HAP-0_{et}) was used as a standard.

The morphology of the formed nanocrystals was studied by transmission electron microscopy Jeol JEM-1011B transmission electron microscope, Japan, resolution 0.3 nm). In addition, some samples were studied by high-resolution transmission electron microscopy on a Jeol JEM-2100 F microscope with the possibility of local energy dispersive X-ray analysis. The samples for transmission electron microscopy were prepared by the deposition on a special copper network with the Formvar droplet of the suspension of the studied crystals diluted with water in a ratio of 30 : 1. Then the samples were dried in air at stored in special pen cases. The size distribution functions of the crystals were obtained using the Image-Pro Plus program.

The contents of zinc and calcium ions in the residual mother liquors after the synthesis were analyzed using the ICP-AES method as indicated above.

MTT test. The procedure of MTT test used for the determination of drug cytotoxicity and LC_{50} evaluation was described in detail.[21] The following cell lines were studied: L-60 (acute promyelocytic leukemia), K-562 (chronic granulocitic leukemia in the blast crisis stage), MOLT-4 (acute T-lymphoblastic leukemia), and MOLT-4 (res) (acute T-lymphoblastic leukemia, line resistant to asparaginase). The samples of all experimentally obtained suspensions were placed (20 mL) each in penicillin glass vials, closed with caps, and sealed with a seaming machine. Then the vials were sterilized (40 min at 110 °C in a drying box), and the samples were subjected to the MMT test.

Results and Discussion

The experiments gave white aqueous suspensions characterized by sedimentation stability. A suspension of HAP-Zn_2 turned out to be most resistant to sedimentation. It can be assumed that the particles forming its solid phase are smaller than those in other samples. The content of the solid phase in the suspensions was (wt.%): HAP-0, 5.5; HAP-0_{HT}, 5.6; HAP-Zn_1, 5.25; and HAP-Zn_2, 6.62. An analysis of the mother liquor showed that $6.35 \cdot 10^{-4}$ % Ca of the weight of all the Ca introduced and $2.83 \cdot 10^{-5}$ % Zn of the weight of all the zinc introduced remained in the solution after the synthesis of the HAP-Zn_1 sample, whereas for the HAP-Zn_2 sample these contents were $5.56 \cdot 10^{-4}$ % Ca and $3.45 \cdot 10^{-5}$ % Zn. Thus, almost the whole zinc introduced into the experiment is captured by the solid phase.

X-ray phase analysis (XRD). The obtained XRD patterns are presented in Fig. 2. The XRD patterns of the

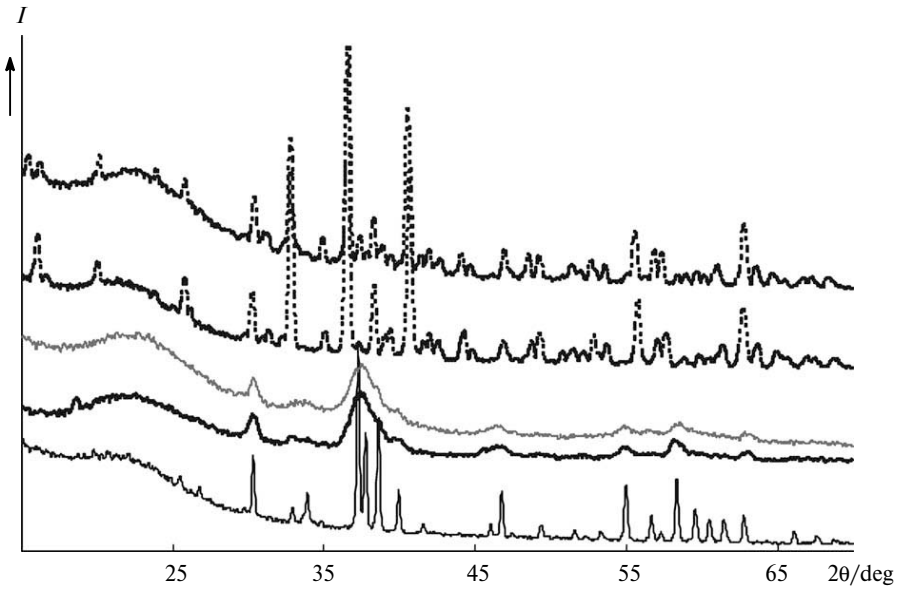

Fig. 2. XRD patterns of the standard HAP-0_{et} sample (*1*) and experimental samples HAP-Zn_1 (*2*), HAP-Zn_2 (*3*), HAP-Zn_{2T} (*4*), and HAP-Zn_{1T} (*5*).

HAP-0 and HAP-0_{HT} samples (not shown in Fig. 2) are nearly identical by the peak positions and widths to those of the diffraction pattern of the basis sample HAP-0_{et} (*1*), which confirms applicability of this synthesis procedure. The XRD patterns of the HAP-Zn_1 (*2*) and HAP-Zn_2 (*3*) samples are also identical to that of HAP-0_{et} (*1*) y the positions of the major peaks. However, the widths of the major peaks increases. The peak broadening increases on going from HAP-Zn_1 to HAP-Zn_2. This indicates the possible formation of finer particles or particles with a lower crystallinity than those of pure HAP in the case of HAP-Zn_1 and HAP-Zn_2. No peaks of the foreign phase were observed. This fact is consistent with the most part of literature data.[16—18,22]

The high temperature treatment conducted to increase crystallinity of the HAP samples with zinc changes the positions of the major peaks relative to the standard sample. An analysis of the positions of major peaks in the XRD patterns showed that they were assigned to the structure β-tricalcium phosphate (β-TCP) with an impurity of the HAP phase. Possibly, upon the thermal action the amorphous-like structure of $Ca_{5-x}Zn_x(PO_4)_3(OH)$ is rearranged to structure β-$Ca_{3-x}Zn_x(PO_4)_2$ (Fig. 3). The probbility of this process is indicated in published works.[17,18,23] An increase in the fraction of zinc in the sample results in a greater rearrangement of the structure and a decrease in the fraction of the primary phase in the drug.

Morphological analysis. The TEM images showing the morphology of the obtained nanocrystals are presented in Fig. 4. Their analysis showed a substantial change in the morphology of the HAP particles upon the introduction of zinc ions or after thermal treatment. The presence of amorphized particles in the HAP-Zn_1 and HAP-Zn_2 samples was confirmed (Fig. 5), which can indicate the ability of zinc ions to inhibit HAP crystallization. This has been indicated previously.[22] The integral distribution functions for the crystal length and width were constructed on the basis of the morphological analysis results (Fig. 6), and the average lengths and widths of the crystals were calculated for each sample (Table 1). It follows from them that crystal width in Zn-HAP decreases compared to pure HAP with an insignificant change in the length. Many amorphized particles with the sizes smaller than those of the major crystals are observed for the HAP-Zn_2 sample. Possibly, this is related to a higher sedimentation stability of the suspension of the crystals considered. Recrystallization (aging) occurs upon the hydrothermal treatment of the starting suspension of HAP-0, after which the nanoplates gain more regular, isomeric shape and become denser (the thickness of the crystal increases and the electron density of the image regularly increases), but the length and width of the nanoplates decrease substantially.

A high-resolution transmission electron microscope combined with the method of local energy dispersive X-ray analysis was used to reveal how uniform is the distribution

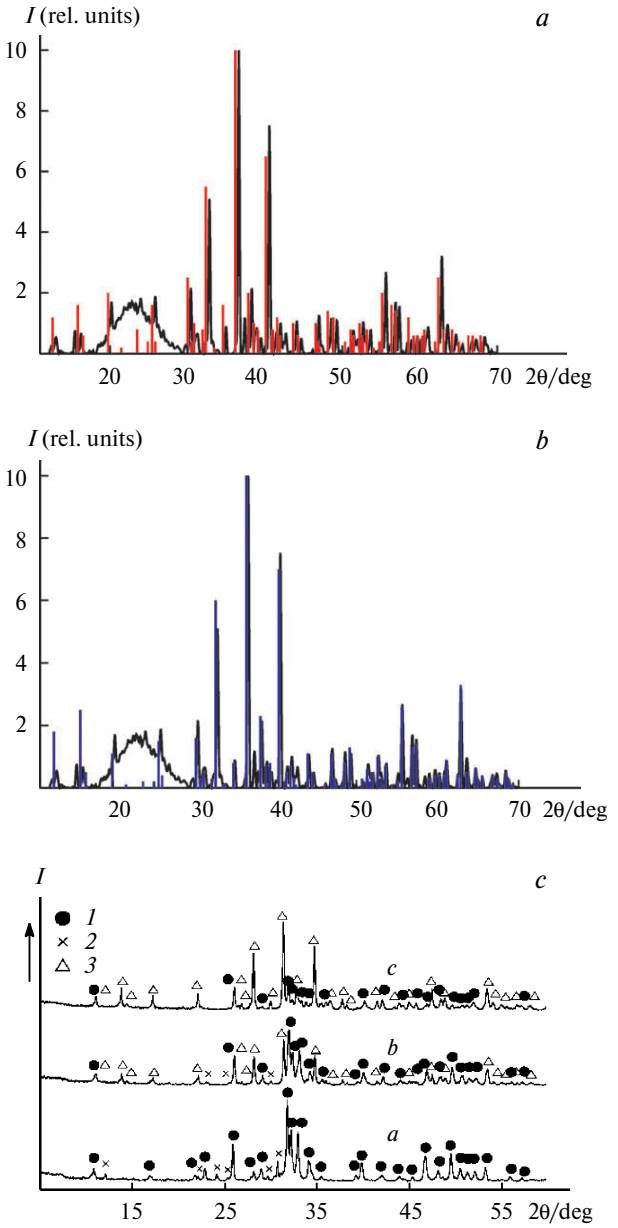

Fig. 3. Decoding of the XRD pattern for the HAP-Zn_{2T} sample: *a*, coincidences of the experimental lines and tabulated lines for β-$Ca_3(PO_4)_2$ (red strokes, ICDD: 00-009-0169); *b*, coincidences of the experimental lines and tabulated lines for $Ca_{19}Zn_2(PO_4)_{14}$ (blue strokes, ICDD: 00-048-1196); *c*, published data[23] showing a change in the structure of the HAP-Zn composites depending on the zinc content after calcination at 800 °C (1 h): 0 (*a*), 5 (*b*), and 10 mol.% (*c*); HAP (*1*), α-TCP (*2*), and β-TCP (*3*).
Note. Fig. 3 is available in full color on the web page of the journal (http://www.link.springer.com).

of the zinc ions over the HAP nanocrystals and whether they form an intrinsic phase or adsorption clusters similar to those observed upon the introduction of iron(III) ions into the synthesis of HAP.[20] It is established that zinc forms no intrinsic phase but is present in all samples in the

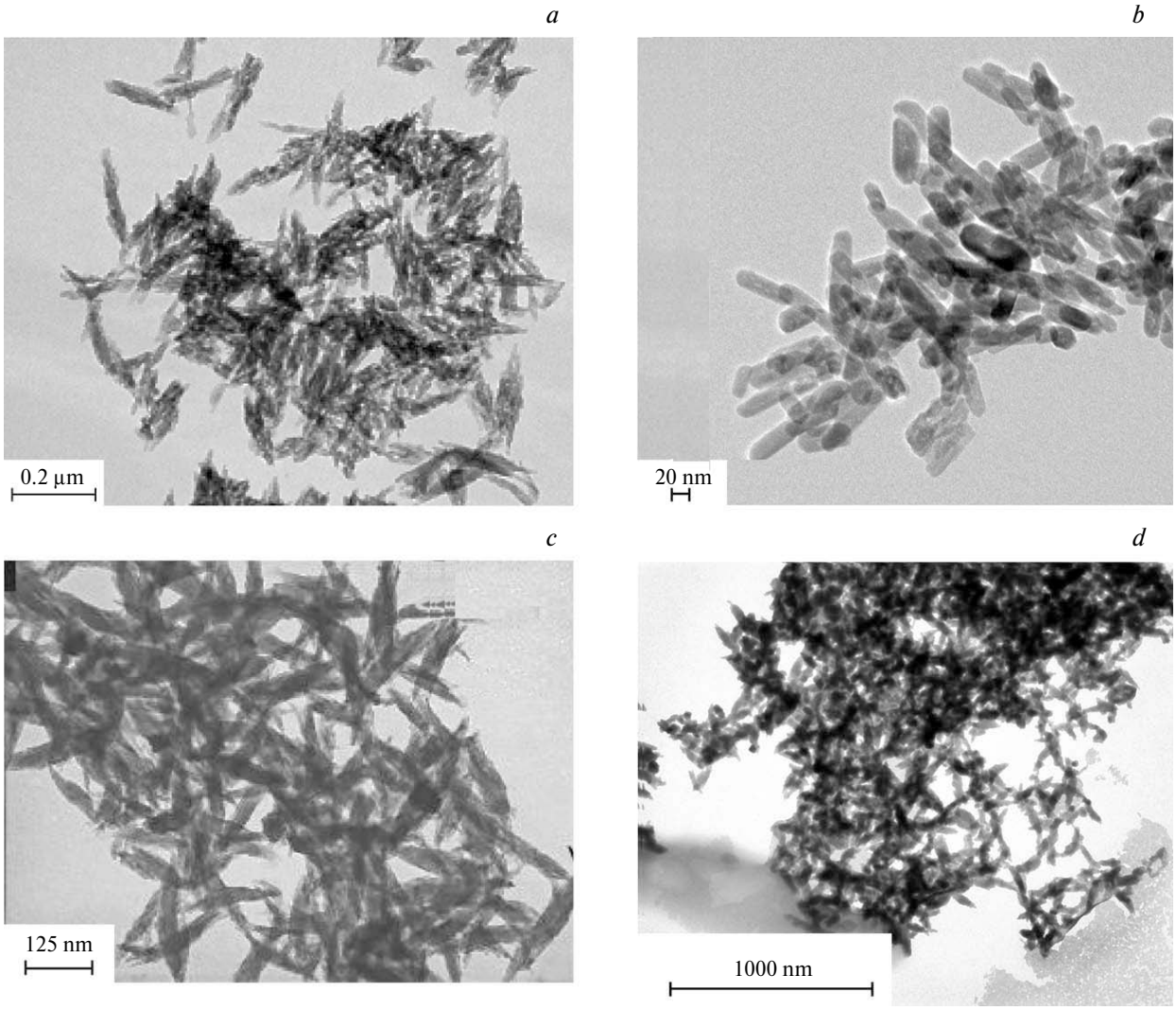

Fig. 4. TEM images of HAP-0 (*a*), HAP-0_{HT} (*b*), HAP-Zn_1 (*c*), and HAP-Zn_2 (*d*).

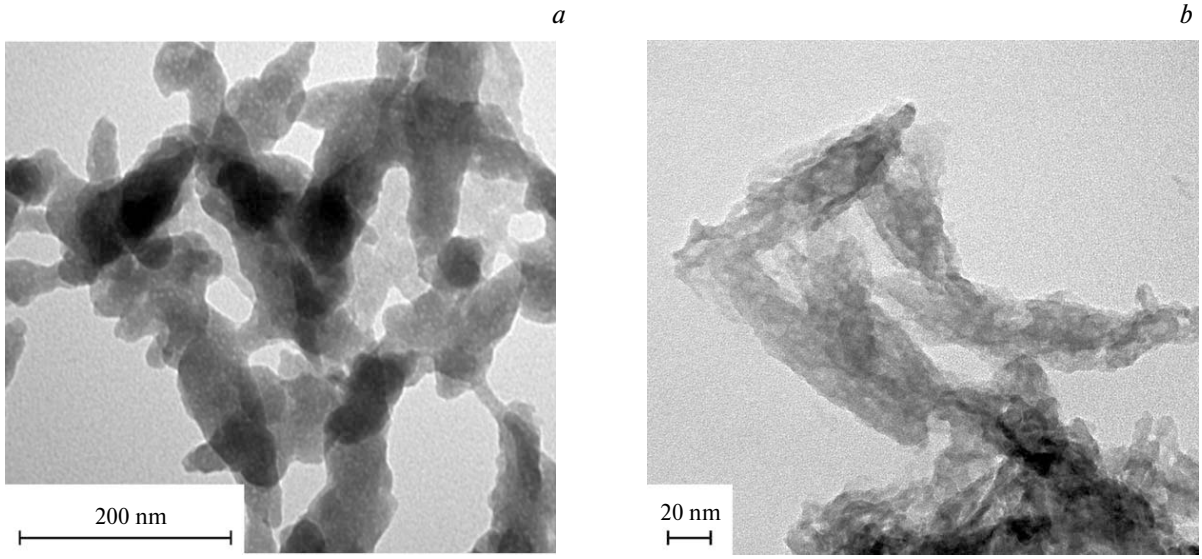

Fig. 5. Amorphized particles in the HAP-Zn_2 sample according to the data of standard transmission electron microscopy (*a*) and high-resolution TEM (*b*).

Table 1. Average sizes of nanoparticles formed in experiments

Nanoparticle	Length	Width
	nm	
HAP-0	120±5	36±3
HAP-Zn_1	110±5	23±2
HAP-Zn_2	98±4	26±2
HAP-0_{HT}	56±2	19±1

amount nearly coinciding with the introduced amount (Fig. 7). The mapping of an agglomerate of HAP-Zn_2 crystals by the contents of the major elements (O, P, Ca, and Zn) showed that the zinc ions are uniformly distributed over the whole agglomerate surface similarly to other elements.

MTT test. The results of the MTT test are presented in Table 2. As can be seen, all HAP samples exhibit a very low cytotoxicity. In the case of HAP-Zn_2, a decrease in the probability of cell survival is observed at a considerable concentration of the drug and, hence, at a high zinc content. This is probably related to the intrinsic toxicity of zinc when it leaves the HAP structure.

Thus, all prepared samples of HAP can act as noncytotoxic spacers for drugs and radiopharmaceuticals. The introduction of zinc ions in the synthesis of HAP results, as can be seen, in their uniform distribution over the HAP

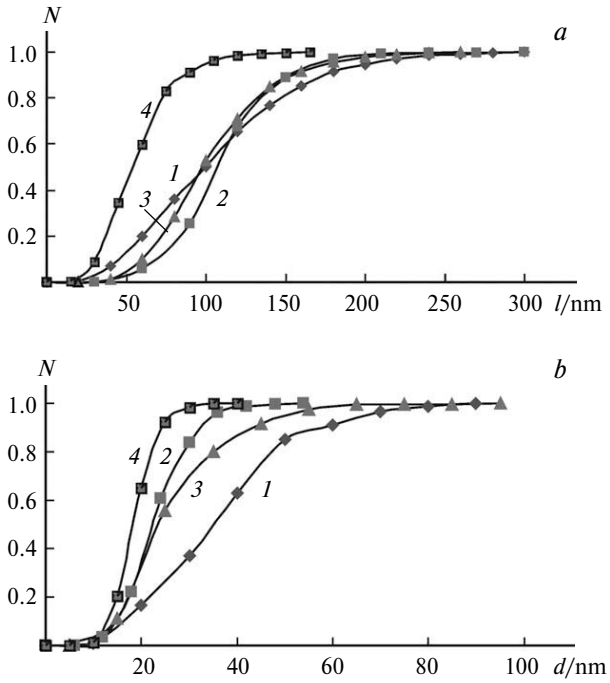

Fig. 6. Integral distribution functions for the length (*l*) (*a*) and width (*d*) (*b*) for crystals of HAP-0 (*1*), HAP-Zn_1 (*2*), HAP-Zn_2 (*3*), and HAP-0_{HT} (*4*).

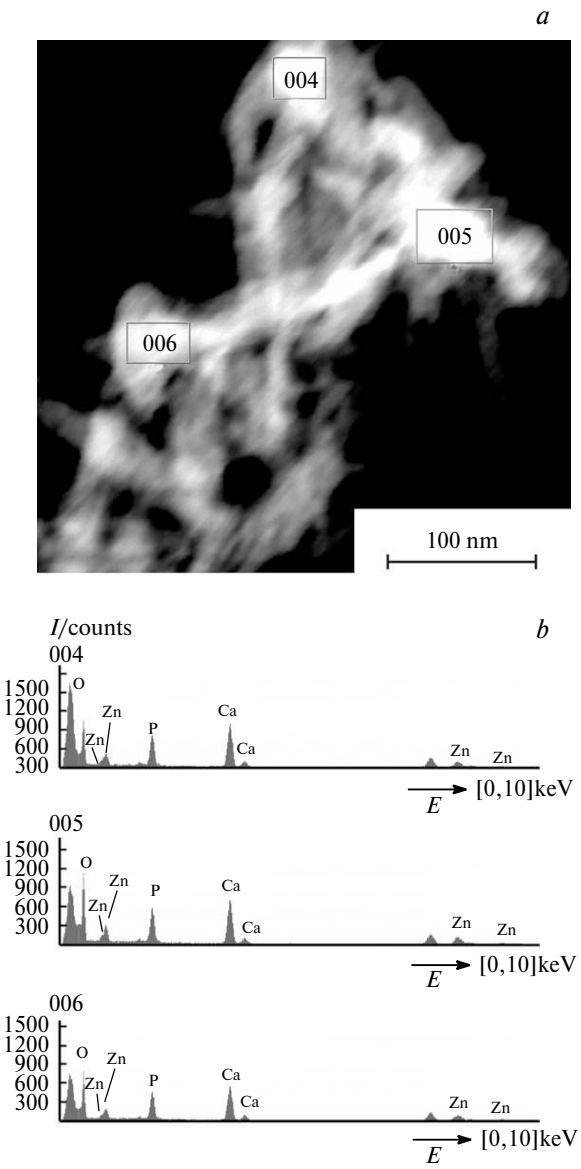

Fig. 7. Results of local energy dispersive X-ray analysis of a suspension of HAP-Zn_2: (*a*) TEM image of aggregates of HAP-Zn_2 nanocrystals and the regions of this object chosen for local analysis; (*b*) analysis results (the observed elements are marked automatically by the processing program).

Table 2. Cytotoxicity (LC_{50}) of the zinc-containing HAP samples

Sample ГАП	LC_{50}/μmol mL^{-1} on various cell lines			
	HL-60	K-562	MOLT-4	MOLT-4 (res)*
HAP	—	>2	3.5	>5
HAP-Zn_1	>5	>5	>5	>5
HAP-Zn_2	3.5	>5	>5	>5
HAP_{HT}	—	>5	4	7

* Cell line resistant to asparaginase.

Table 3. Comparison of ionic radii of zinc and calcium ions

Ion	Radius/nm		
	by Goldschmidt	by Pauling	by Belov and Bokii
Ca^{2+}	0.106	0.098	0.104
Zn^{2+}	0.083	0.074	0.082

structure, affects the structure of HAP, and exert different effect of cytotoxicity. Zinc can substitute calcium in its crystallographic positions with the coordination number six.[17] A comparison of sizes of zinc and calcium ions (Table 3) showed that for a similar substitution the starting HAP structure is distorted but this distortion is not almost observed in the XRD patterns of the samples because of very broad peaks of the major substance. An increase in the concentration of zinc ions results in the inhibition of crystallization of mixed phosphate and formation of the amorphized product with a change in the morphology and sizes of the crystals. The high-temperature treatment of the obtained samples at 900 °C changes the structures of mixed phosphate from the apatite-like structure to the structure of the β-TCP (tricalcium phosphate) type.

The authors are grateful to the Research and Educational Center of Collective Use "Nanochemistry and Nanomaterials" at the M. V. Lomonosov Moscow State University for help in studying morphology of the samples.

This work was financially supported by the Russian Foundation for Basic Research (Project No. 16-08-00139).

References

1. Y. Lee, Y. Lin, C. Lima, *J. Chin. Chem. Soc.*, 2014, **61**, 142.
2. P. X. Ma, *Adv. Drug Deliv. Rev.*, 2008, **60**, 184.
3. D. W. Hutmacher, J. T. Schantz, C. X. F. Lam, K. C. Tan, T. C. Lim, *J. Tissue Eng. Regenerative Med.*, 2007, **1**, 245.
4. M. P. Ferraz, F. J. Monteiro, C. M. Manuel, *J. Appl. Biomater. Biomechanics*, 2004, **2**, 74.
5. F. Sun, H. Zhou, J. Lee, *Acta Biomaterialia,* 2011, **7**, 3813.
6. G. Wei, P. X. Ma, *Adv. Funct. Mater.*, 2008, **18**, 3568.
7. Y. Huang, G. Zhou, L. Zheng, H. Liu, X. Niu, Y. Fan, *Nanoscale*, 2012, **4**, 2484.
8. M. Jarcho, *Dent. Clin. North. Am.*, 1992, **36**, 19.
9. M. Tirrell., E. Kokkoli, M. Biesalski, *Surf. Sci.,* 2002, **500**, 61.
10. X. Zhu, O. Eibl, C. Berthold, L. Scheideler, J. Geis-Gerstorfer, *Nanotechnology*, 2006, **17**, 2711.
11. B. Sridevi, J. P. G. Eddy, F. Derek*, Am. J. Mater. Sci.*, 2015, **5**, 32.
12. A. V. Severin, N. I. Silkin, L. F. Galiullina, O. N. Mazaleva, V. N. Rudin, M. Kh. Salakhov, R. N. Khairullin, Yu. A. Chelyshev, *Uch. Zap. Kazan. Un-ta* [*Scientific Writings of Kazan Univ.*], 2012, **145**, 127 (in Russian).
13. I. V. Melikhov, V. F. Komarov, A. V. Severin, V. E. Bozhevol´nov, V. N. Rudin, *Dokl. Akad. Nauk*, 2000, **373**, 355 [*Dokl. Chem.* (*Engl. Transl.*), 2000].
14. F. S. Fomin, V. S. Komlev, S. M. Barinov, I. V. Fadeeva, K. Rengini, *Perspekt. Mater.* [*Perspective Materials*], 2006, No. 2, 51 (in Russian).
15. E. V. Safronova, V. I. Putlyaev, A. I. Sergeeva, E. V. Kunenkov, Yu. D. Tret´yakov, *Dokl. Akad. Nauk*, 2009, **426**, 491 [*Dokl. Chem.* (*Engl. Transl.*), 2009].
16. E. S. Thian, T. Konishi, Y. Kawanobe, P. N. Lim, C. Choong, B. Ho, M. Aizawa, *Mater. Med.,* 2013, **24**, 437.
17. Y. Tang, H. F. Chappell, M. T. Dove, R. J. Reeder, Y. J. Lee, *Biomaterials,* 2009, **30**, 2.
18. K. P. Tank, K. S. Chudasama, V. S. Thaker, M. J. Joshi, *J. Cryst. Growth*, 2014, **401**, 474.
19. X. Yuping, W. Franklin, W. Schwartz, J. Samuel, S. Traina, *Envir. Sci. Technol.*, 1994, **28**, 8.
20. A. V. Severin, D. A. Pankratov, *Zh. Neorg. Khim.*, 2016, **61**, 1 [*Russ. J. Inorg. Chem.* (*Engl. Transl.*), 2016, **61**].
21. M. A. Orlova, E. Yu. Osipova, S. A. Roumiantsev, *Br. J. Med. Med. Res.,* 2012, **2**, 21—30.
22. A. Bigi, E. Foresti, M. Gandolfi, M. Gazzano, N. Roveri, *J. Inorg. Biochem.*, 1995, **58**, 49.
23. F. Miyaji, Y. Kono, Y. Suyama, *Mat. Res. Bull.*, 2005, **40**, 209.
24. W. H. Elliott, D. C. Elliott, *Biochemistry and Molecular Biology*, 2nd ed., Oxford University Press, Oxford, 2001.

Received June 16, 2016;
in revised form November 3, 2016